Morphing Concept for Multirotor UAVs Enabling Stability Augmentation and Multiple-Parcel Delivery

Damian Cheng*, Aravinda C. Charles†, Sutthiphong Srigrarom‡, and Henrik Hesse§

University of Glasgow Singapore, 510 Dover Road, 139660 Singapore

This paper presents a novel morphing concept for multirotor Unmanned Aerial Vehicles (UAVs) to optimize the vehicle flight performance during multi-parcel deliveries. Abrupt changes in the vehicle weight distribution during a parcel delivery can cause the UAVs to be unbalanced. This is usually compensated by the vehicle flight control system but the motors may need to operate outside their design range which can deteriorate the stability and performance of the system. Morphing the geometry of a conventional multirotor airframe enables the vehicle to continuously re-balanced itself which improves the overall vehicle performance and safety. The paper derives expressions for the static stability of multirotor UAVs and discusses the experimental implementation of the morphing technology on a Y6 tricopter configuration. Flight test results of multi-parcel delivery scenarios demonstrate the capability of the proposed technology to balance the throttle outputs of all rotors.

I. Introduction

Technology innovations in Unmanned Aerial Vehicles (UAVs) have driven their increasing application in a range of industries. As one such application, delivery drones are of particular interest for the near future with logistic and online retail companies such as Amazon and UPS planning to launch fleets of aerial delivery drones. Figure 1b shows an example of a commercial delivery drone which has been demonstrated for last mile delivery of single parcels. Recent improvements in UAV technology have further contributed to increased payload capacity, extended operating range, and autonomous last mile delivery making such concepts of delivery drones viable products.[1] Such improvements allow future delivery drones to process more than a single parcel which can increase coverage by eliminating multiple flights to complete the same task. The concept of multi-parcel delivery therefore significantly reduces delivery cost and time.

The major hurdle in the development of a platform with multi-payload capability is the abrupt change in Center of Gravity (CG). In the design of Multirotor UAVs (M-UAVs), such as the examples shown in Fig. 1, balancing the weight of the vehicle and its payload is crucial. Unlike fixed-wing aircraft, M-UAVs achieve stable and efficient flight when the moments generated by the mass distribution (CG location) is in equilibrium with the moments generated by the thrust from all rotors. The latter is commonly defined as Neutral Point (NP) in flight mechanics of fixed-wing aircraft[2] which can be defined for M-UAVs as the location on the vehicle where the moments from all propulsion forces balance to zero. Balancing the weight distribution is also crucial for the next generation of urban transportation using Personal Aerial Vehicles (PAVs) such as the concept shown in Fig. 1a.[3] The envisioned passenger drone has an empty weight of 240 kg and is designed for two people with a total payload capability of 120 kg. Hence, the CG location would significantly shift along the longitudinal axes depending on the occupancy (one or two passengers). Such offsets are usually compensated by the vehicle Flight Control System (FCS).

Depending on the level of autonomy, M-UAVs are typically equipped with flight control units to (a) guide the drone to follow specific waypoints and (b) stabilize the vehicle around a specific attitude. Even if the vehicle is piloted manually, all commercial M-UAVs usually include such stabilizing controller which tracks

*Research Student, Aerospace Division.
†Research Student, Aerospace Division.
‡Associate Professor, Aerospace Division, AIAA Member.
§Assistant Professor, Aerospace Division, AIAA Member. Corresponding author: henrik.hesse@glasgow.ac.uk

(a) Amazon Prime Air (`amazon.com/primeair`)

(b) Elroy Passenger Drone (`flyastro.com`)

Figure 1: Concepts of aerial vehicles for (a) parcel delivery and (b) passenger transportation.

the pilot inputs of commanded attitude angles for roll, pitch, and yaw. In hover, for example, the FCS aims to maintain an equilibrium by holding a specific position and attitude.[4–6]

Hence, the FCS is able to compensate for small offsets in the CG location in off-balanced designs by increasing the motor throttle output to re-balance all moments acting on the M-UAV.[7] However, a critical limitation to delivering multiple parcels using M-UAVs is the detrimental flight behavior due to the unbalanced CG position. For conventional M-UAVs the vehicle frame is fixed and, if the weight is not balanced correctly, the motors are commanded by the FCS to operate outside their design range which can affect the vehicle flight time and stability of the system. In this work we therefore propose a morphing concept to change the frame configuration of the vehicle which allows corrections of the CG balance.

The proposed concept of morphing a M-UAV comprises of altering the geometry of a multirotor vehicle by adjusting the angle between the motor arms. By symmetric sweeping of the motor arms, the change in angles between the arms not only changes the CG location of the vehicle frame but also affects the NP along the longitudinal direction of the M-UAV where all moments balance to zero. This opens the possibility of re-balancing the drone in case of variable CG positions to maintain balanced throttle outputs to all rotors. The latter is key to ensuring operation of all rotors within their optimal speed range which enhances the vehicle flight characteristics with regards to its stability and flight endurance. Note that the vehicle dynamics can also be stabilized by moving the CG location, for example, by shifting the payload or batteries, which will not be addressed in this work.

The concept of morphing is not new and has been explored for manned and unmanned fixed-wing aircraft for decades to enhance vehicle flight performance through improved aerodynamic performance during different phases of flight, extended operating range, endurance and wide variation of mission profiles for a single aircraft.[8,9] For fixed-wing UAVs such changes in the longitudinal dynamic modes have been shown by sweeping of the main wings.[10]

Although morphing has been studied extensively for fixed-wing aircraft, there is a lack of research in morphing a multirotor vehicles to improve its handling qualities and efficiency. Recently, a dynamic morphing approach has been applied to quadrocopter to be able to maneuver through small gaps.[11] Instead, in this work we propose a morphing concept of the UAV frame to ensure static stability for safe and efficient operation of M-UAVs in the expanding aerial robotics community. As an example for the proposed technology, this work demonstrates how morphing for M-UAVs can enable the delivery of multiple parcels without penalizing the vehicle flight performance.

By applying the notion of static stability to M-UAVs in hover, this work analyzes the effect of balancing, as the relation between the vehicle CG and NP locations, on the overall vehicle flight performance. Although the modeling of quadrocopters and the dynamic stability derivatives have been explored previously,[12] it is crucial to include the maximum available thrust from all rotors in the stability analysis to obtain a measure of the vehicle static margins. Based on the measures of static margins for conventional M-UAVs, we further evaluate the improved stability of the proposed morphing concept in theory and through experimental results. The proposed morphing technology can be combined with existing off-the-shelf FCS and the paper proposes

a cascaded control approach to control the morphing mechanism in flight and achieve continuous neutral stability of the M-UAV during multi-parcel delivery.

II. Concept of Multirotor Morphing

In this section we propose the concept of morphing for multirotor vehicles for multi-parcel scenarios leading to off-balanced drone configurations. To evaluate the benefits of the morphing strategy to improve the vehicle flight performance, this section also explores the static stability characteristics of conventional M-UAVs without morphing and extends the theory to vehicles with morphing capabilities.

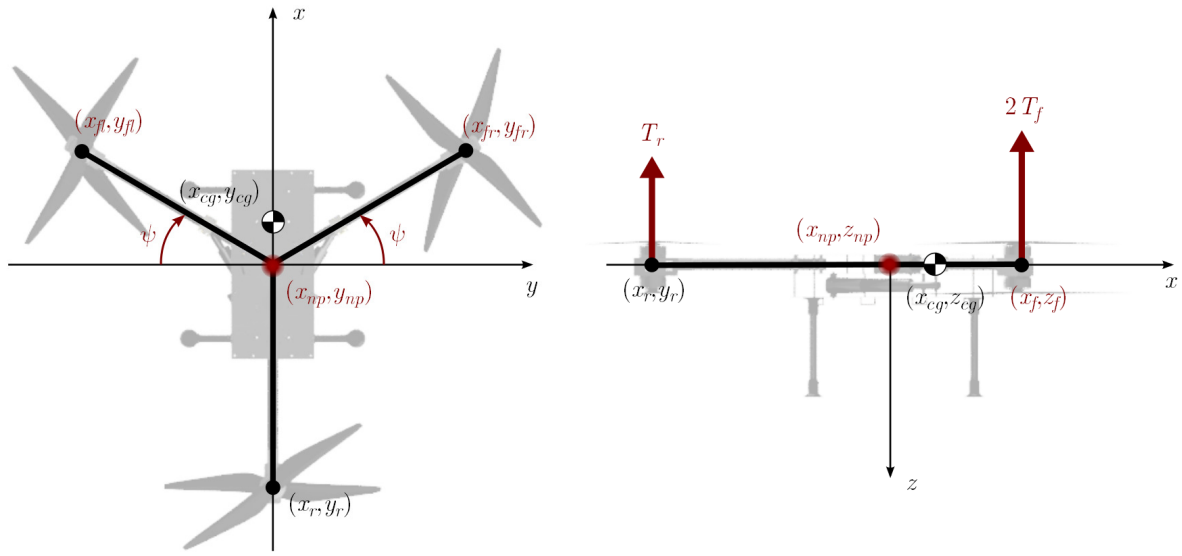

(a) top view

(b) side view

Figure 2: Definition of the co-axial Y6 tricopter configuration with sweep angle ψ and location of the vehicle neutral point $(x_{np},\ y_{np},\ z_{np})$ and center of gravity $(x_{cg},\ y_{cg},\ z_{cg})$.

A. Airframe Configuration of Multirotor Morphing Platform

To develop the proposed morphing concept, we focus on a coaxial Y6 tricopter configuration as illustrated in Fig. 2. The configuration consists of three arms with equal arm length l and pairs of coaxial rotors mounted at the ends of each arm. For conventional Y-shaped tricopters the arms are spaced 120° apart, however, by sweeping the front two arms of the tricopter, it is possible to morph from a Y to T-shaped configuration as illustrated in Fig. 3 for different sweep angles ψ. Note that in this work we only consider longitudinal problems of tricopter configurations and we assume the sweeping of the left and right motor arms to be symmetric, as specified in Tab. 1. The morphing concept however can be extended to conventional quadrocopter vehicles and lateral problems.

Table 1: Longitudinal definition of coaxial Y6 tricopter configuration as shown in Fig. 2 where the length of rotor arm is l and the configuration is assumed to be symmetric in $x-z$ plane and restricted to $x-y$ plane.

Coaxial rotor i	Position $[x_i,\ y_i,\ z_i]^T$	Thrust vector
Front left	$[l\sin\psi,\ -l\cos\psi,\ 0]^T$	$[T_f,\ 0,\ 0]^T$
Front right	$[l\sin\psi,\ l\cos\psi,\ 0]^T$	$[T_f,\ 0,\ 0]^T$
Rear	$[-l,\ 0,\ 0]^T$	$[T_r,\ 0,\ 0]^T$

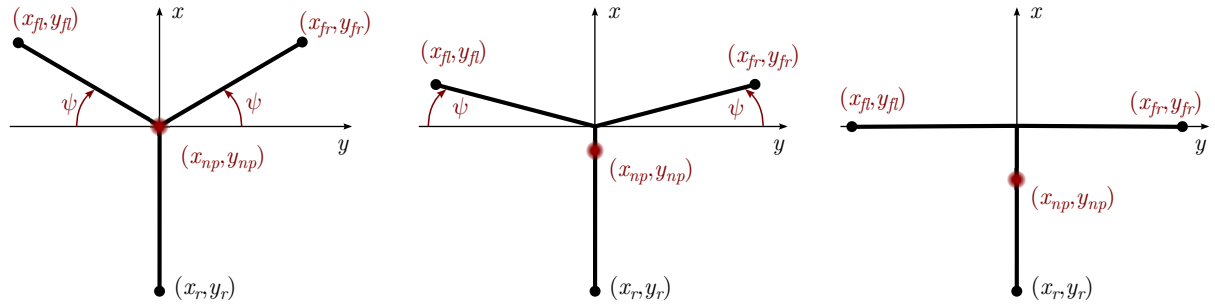

(a) $\psi = 30°$ (b) $\psi = 15°$ (c) $\psi = 0°$

Figure 3: Transition from Y to T tricopter configuration by morphing rotor arms through sweep angle ψ.

1. *Effect of Morphing on Moment Distribution*

As illustrated in Figs. 2-3 by the red circle, sweeping from a Y to T configuration causes the neutral point (NP) of the vehicle to shift backwards towards the rear rotor. Here, we lend the term neutral point from traditional fixed-wing flight dynamics[2] and apply it to multirotor vehicles, whereby the neutral point $[x_{np},\ y_{np},\ z_{np}]^T$ defines the location on the vehicle where the moments from the all external forces balance to zero, e.g. along the x-axis

$$\sum_i (x_i - x_{np})T_i = 0 \tag{1}$$

with x_i being the location where the force T_i is applied. For the Y configuration, as shown in Fig. 2, we only consider the thrust forces from the two front rotors (each coaxial front rotor produces T_f) and the rear rotor (T_r) as external forces. The neutral point location along the x axis is then given as,

$$x_{np} = \frac{2T_f x_f + T_r x_r}{2T_f + T_r}. \tag{2}$$

Using the definition of rotor locations and assumptions given in Tab. 1, we can express the location of the neutral point in non-dimensional form by normalizing with the length of the rotor arms l, such that

$$\bar{x}_{np} = \frac{x_{np}}{l} = \frac{2T_f \sin\psi - T_r}{2T_f + T_r}. \tag{3}$$

Hence, assuming constant throttle outputs, Eq. (2) confirms the notion that the sweeping from a Y to T configuration causes the neutral point of the vehicle to shift backwards towards the rear rotor. This shift of the NP location forms the motivation for the morphing concept to improve stability of multirotor vehicles, for example, due to disturbances or balancing issues following the delivery of multiple parcels.

2. *Multi-parcel Delivery Scenario*

Figure 4 illustrates the challenges in the design of a multi-parcel delivery vehicle. For the balanced configuration shown in Fig. 4a all payload bays are filled equally such that the CG of the combined payload coincides with the CG of the empty vehicle along the x axis,

$$x^0_{cg} = \frac{M_e x^e_{cg} + M_p x^p_{cg}}{M_{TOW}}, \tag{4}$$

where $M_{TOW} = M_e + M_p$ is the total mass of the UAV with the vehicle empty mass M_e lumped at x^e_{cg} and combined payload mass M_p lumped at x^p_{cg}. Hence, for the balanced loading configuration in Fig. 4a we have $x^0_{cg} = x^e_{cg} = x^p_{cg}$.

However, during a multi-parcel delivery mission, the M-UAV can have very different stability characteristics at every phase of the mission profile due to the change in weight distribution when a parcel is delivered. Figure 4b illustrates how the overall CG location x_{cg} changes due to an unbalanced loading scenario. Hence,

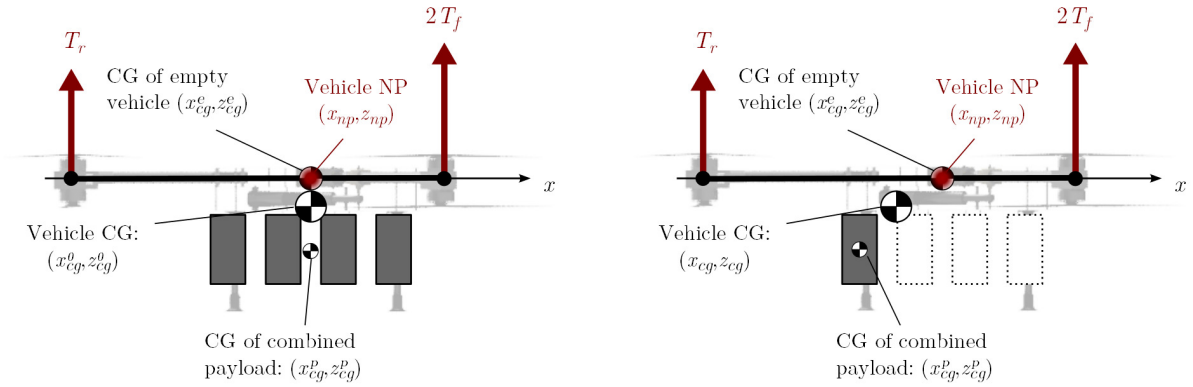

(a) Fully filled configuration.

(b) Only one payload bay filled.

Figure 4: Concept of multi-parcel delivery drone with four payload bays (gray indicating full bays). The neutral point (NP) location shown in red and the locations of the center of gravity (CG) of the empty vehicle configuration, the combined payload, and complete vehicle is also shown.

after delivery of the three front parcels, the overall CG location shifts by Δx_{cg} from the balanced CG location, x^0_{cg}, such that

$$x_{cg} = x^0_{cg} + \Delta x_{cg} = \frac{M_e x^e_{cg} + M_p \left(x^p_{cg} + \Delta x^p_{cg}\right)}{M_{TOW}}, \tag{5}$$

where Δx^p_{cg} is the offset of the combined payload CG with respect to the balanced CG of the vehicle. We find that the resulting CG for the unbalanced vehicle is shifted by

$$\Delta x_{cg} = \frac{M_p}{M_{TOW}} \Delta x^p_{cg} \tag{6}$$

and the vehicle shown in Fig. 4b becomes tail-heavy. On conventional M-UAVs, the vehicle frame is fixed and the CG offset Δx_{cg} is usually compensated by the flight controller by increasing the motor throttle output at the rear to re-balance all moments acting on the M-UAV.[7] Power is therefore wasted merely to balance the vehicle which reduces the available excess power to maneuver and stabilize the vehicle. This will be discussed in the next section.

B. Longitudinal Static Stability for Multirotor Vehicles in Hover

Since multirotor vehicles typically have no lifting surfaces to produce lift and restoring forces due to pitch disturbance, as would be the case for fixed-aircraft, the UAV is balanced only through thrust from the rotors in a closed-loop fashion. However, in this section we aim to adopt the concept of static stability from fixed aircraft and apply it to multirotor vehicles such as the configuration shown in Fig. 2.

Assuming the M-UAV to be in perfect hover condition, the thrust from all three rotors balances the total take-off weight of the vehicle, M_{TOW}, which constraints the throttle outputs such that

$$F_{TOW} = M_{TOW} \cdot g = 2T_f + T_r \tag{7}$$

where g is the gravitational acceleration. Assuming all rotors to be identical and the vehicle to be perfectly trimmed, i.e. the CG of the vehicle coincides with the NP such that $\bar{x}^0_{cg} = \bar{x}^0_{np}$ for the balanced vehicle, each rotor produces the same thrust with $T_f = T_r = T^0$ and $F_{TOW} = 3T^0$.

However, as illustrated in Fig. 4b, during a multi-parcel delivery scenario the CG location may shift by Δx_{cg} away from the NP position x_{np}, which is compensated by the flight control system leading to differences in thrust inputs between front and rear rotors, i.e. $T_r = T^0 + \Delta T_r$ and $T_f = T^0 + \Delta T_f$. Hence, the non-dimensional form of the NP location in Eq. (3) changes in the closed-loop case to

$$\bar{x}_{np} = \bar{x}^0_{np} + \Delta \bar{x}_{np} = \frac{2\left(T^0 + \Delta T_f\right)\sin\psi - \left(T^0 + \Delta T_r\right)}{2\left(T^0 + \Delta T_f\right) + \left(T^0 + \Delta T_r\right)} \tag{8}$$

Table 2: Maximum achievable NP corrections $\Delta\bar{x}_{np}$ normalized with rotor arm length for the different configurations ($\psi = 0°$, 15°, and 30°) in Fig. 3 and different nominal throttle outputs e^0 considering the bound $\left(e^0 + \Delta e\right) \leq 0.65$ on allowable throttle outputs as percentage of maximum thrust per rotor.

e^0	$\psi = 30°$	$\psi = 15°$	$\psi = 0°$
0.4	0.313	0.262	0.208
0.5	0.150	0.126	0.100
0.6	0.042	0.035	0.028

where the flight controller manipulates $\Delta\bar{x}_{np}$ to re-balance the vehicle, i.e. $\Delta\bar{x}_{np} = \Delta\bar{x}_{cg}$, where $\Delta\bar{x}_{cg}$ is the CG offset defined in Eq. (6) normalized by the rotor arm length l. Since the hover condition in Eq. (7) needs to be fulfilled, i.e. constant $F_{TOW} = 2\left(T^0 + \Delta T_f\right) + \left(T^0 + \Delta T_r\right)$, the incremental thrust corrections to front and rear rotors are related as

$$\Delta T_r = -2\Delta T_f = \Delta T, \tag{9}$$

and the closed-loop NP correction in Eq. (8) simplifies to

$$\Delta\bar{x}_{np} = -\frac{\Delta T}{3T^0}\left(\sin\psi + 1\right). \tag{10}$$

To finally link the above derivation to the concept of static stability and predict the possible range of CG offsets that can be compensated by the flight control system, we define the nominal thrust level at hover T^0 and the thrust increment ΔT in terms of percentage throttle outputs (or fractions) of the maximum available thrust at each rotor T^{max} as,

$$e^0 = \frac{T^0}{T^{max}} \quad \text{and} \quad \Delta e = \frac{\Delta T}{T^{max}}. \tag{11}$$

Hence, the maximum achievable correction in NP location from the nominal tricopter design is given as,

$$\Delta\bar{x}_{np} = -\frac{1}{3}\frac{\Delta e}{e^0}\left(\sin\psi + 1\right), \tag{12}$$

which can be manipulated to balance the vehicle in pitch, i.e. for the instantaneous NP location $\bar{x}_{np}$ to match off-balanced CG position $\bar{x}_{cg}$. Hence, the vehicle can be stabilized either through the flight control system by manipulating Δe or through the morphing mechanism proposed in this work by changing ψ. Both methods will be discussed next.

1. Longitudinal Static Stability without Morphing

In the discussion of Eq. (12) for static stability of M-UAVs we first analyze the conventional design of a tricopter *without* morphing. Hence, the sweep angle ψ is constant for the different configurations ($\psi = 0°$, 15°, and 30°) shown in Fig. 3 and the standard flight control system only varies the differential thrust between front and rear rotors, $\Delta T = \Delta e T^{max}$ for a nominal thrust input $T^0 = e^0 T^{max}$, as defined in Eq. (11).

To develop efficient M-UAVs with maximum flight time, the vehicle is designed such that the nominal throttle output e^0 is at the optimal operating point of the selected motors, typically $0.4 \leq e^0 \leq 0.65$.[13] Additionally, we need to introduce a bound on the differential thrust available to balance the CG offsets, where $\left(e^0 + \Delta e\right) \leq 0.65$ is typical for delivery or surveillance vehicles to allow for excess thrust to climb and react to disturbances.[14]

Using Eq. (12) and the typical range for e^0 and $\left(e^0 + \Delta e\right)$, as discussed above, Table 2 presents the achievable NP displacements for the three configurations shown in Fig. 3 to balance the CG offsets Δx_{cg}. For nominal throttle outputs of $e^0 = 0.4$, the flight control system has an excess throttle of 25% to stabilize a CG offset of up to 31% of the arm length l. However, such low trim values e^0 at hover are more characteristic for overpowered racing drones with high maneuverability which requires larger (and heavier) motors and comes at the cost of reduced payload capability and endurance. Hence, hover values of $e^0 = 0.5$ and 0.6 are more appropriate for delivery drones as the concept discussed in detail in Sec. IV. For those more efficient

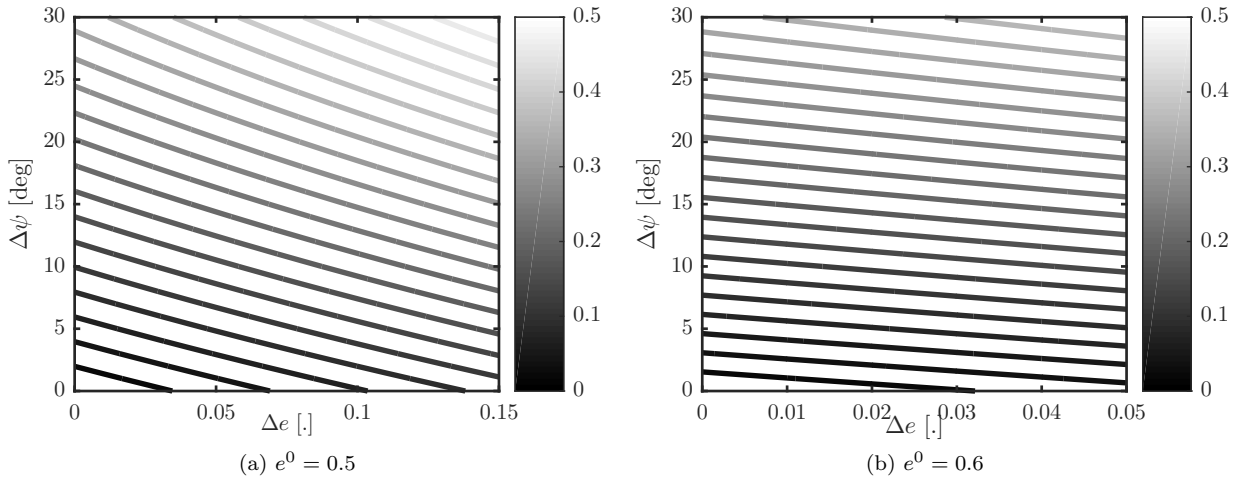

(a) $e^0 = 0.5$ (b) $e^0 = 0.6$

Figure 5: Maximum achievable CG corrections $\left(\Delta\bar{x}_{np}^{\Delta\psi} + \Delta\bar{x}_{np}^{\Delta T}\right)$ normalized with rotor arm length for different nominal throttle outputs e^0 considering the bound $\left(e^0 + \Delta e\right) \leq 0.65$ on allowable throttle outputs as percentage of maximum thrust per rotor.

designs the available margins for CG offsets are maximum 15 and 4%, respectively, of the rotor arm lengths, as shown in Table 2. For a UAV with an arm length of 0.4 m, for example, such margins relate to only 0.02-0.06 m allowable CG offset which is not sufficient for delivery of multiple parcels or to account for small design flaws.

2. Longitudinal Static Stability with Morphing

Even for the Y configuration (cmp. $\psi = 30°$ in Table 2), which provides larger potential margins due to its geometry, a conventional flight control system would not have sufficient margins to correct for large CG offset as may occur during multiple parcel delivery scenarios described in Sec. II.2. Hence, this work proposes a morphing mechanism to control the NP location by manipulating the sweep angle $\psi = \psi^0 + \Delta\psi$ for the configuration shown in Fig. 2.

By substituting $\psi = \psi^0 + \Delta\psi$ in Eqs. (8)-(12), the general expression for the NP location with differential thrust $\Delta T = \Delta e T^{max}$ and morphing $\Delta\psi$ is given as,

$$\bar{x}_{np} = \frac{1}{3}\left[\left(2 - \frac{\Delta e}{e^0}\right)\sin\left(\psi^0 + \Delta\psi\right) - \left(1 + \frac{\Delta e}{e^0}\right)\right]. \tag{13}$$

Without loss of generality, if we assume the nominal configuration of the tricopter to be a T configuration, i.e. $\psi^0 = 0$, we can simplify Eq. (13) such that,

$$\begin{aligned} \bar{x}_{np} = \;& \bar{x}_{np}^0 + \Delta\bar{x}_{np}^{\Delta\psi} + \Delta\bar{x}_{np}^{\Delta T} \quad \text{with} \\ & \bar{x}_{np}^0 = -\frac{1}{3}, \quad \Delta\bar{x}_{np}^{\Delta\psi} = \frac{2}{3}\sin\Delta\psi, \quad \Delta\bar{x}_{np}^{\Delta T} = -\frac{1}{3}\frac{\Delta e}{e^0}\left(\sin\Delta\psi + 1\right), \end{aligned} \tag{14}$$

where $\bar{x}_{np}^0$ is again the nominal NP location with $\Delta\bar{x}_{np}^{\Delta\psi}$ and $\Delta\bar{x}_{np}^{\Delta T}$ expressing the change in NP location due to morphing and differential thrust, respectively, to correct possible CG offsets.

Figure 5 shows the contour plots of achievable NP adjustments $\Delta\bar{x}_{np}^{\Delta\psi}$ and $\Delta\bar{x}_{np}^{\Delta T}$ for different nominal throttle outputs e^0. Even without relying on the flight control system to stabilize the vehicle, i.e. by morphing alone, the proposed concept can achieve NP corrections of 33% of the rotor arm length. Hence, the morphing system has the potential to stabilize the CG offsets similar to the capabilities of the overpowered rigid M-UAV with $e^0 = 0.4$ (cmp. $\psi = 30°$ in Table 2), however, for the morphing vehicle the correction is independent of the nominal throttle output e^0. This can lead to more efficient configurations, as shown in Fig 5b. For a nominal throttle output of 60% at hover, i.e. $e^0 = 0.6$, the flight control system has limited

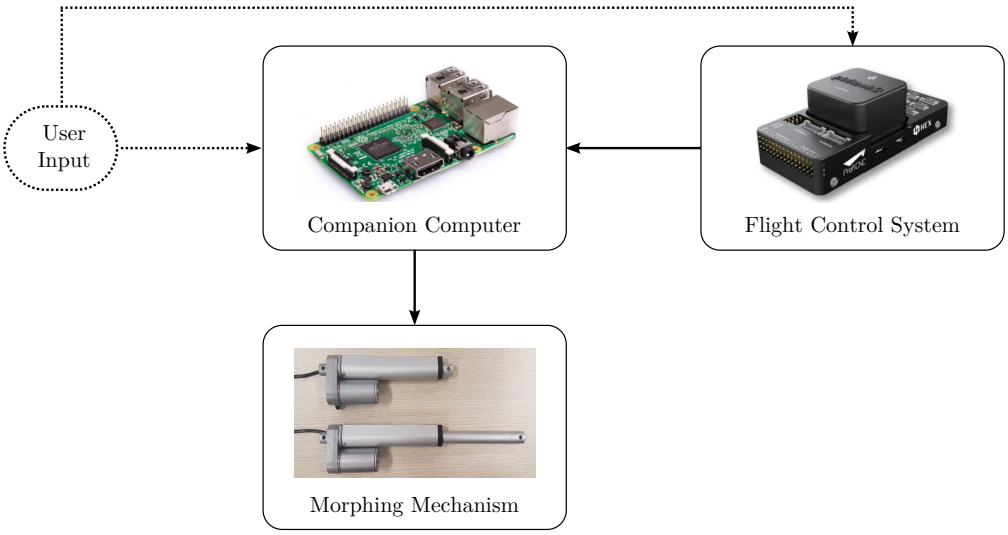

Figure 6: On-board M-UAV software architecture with closed-loop information flow (solid arrows) and open-loop path (dashed lines).

excess throttle output, $\Delta e \leq 0.05$, to correct for the CG offset (cmp. $e^0 = 0.6$ in Table 2), however, the morphing system combined with the flight control system has the potential to correct a CG offset of up to 38% of the rotor arm length even for this underpowered configuration. For the standard design with 50% throttle at hover, i.e. $e^0 = 0.5$, the morphing system combined with the flight control system can correct CG offsets of up to 50% of the rotor arm length. For the proof of concept in this work, as discussed in Sec. IV, the rotor arm length is approx. 0.4 m which allows offsets in the vehicle CG locations of up to 0.2 m.

III. Stability Augmentation System with Multirotor Morphing

Most M-UAVs rely on on-board flight control systems (FCS) to stabilize the vehicle around reference conditions determined either by a guidance algorithm or pilot inputs. In this section we illustrate the extension of such off-the-shelf FCS to enable the integration of a morphing controller to stabilize the vehicle more efficiently in addition to the standard FCS.

A. System Architecture

In this work we use the off-the-shelf Pixhawk control platform which contains an embedded processor to run the flight control software PX4 and several sensors for state estimation. The PX4 autopilot firmware is an open-source software architecture, which integrates modules for guidance, navigation, and control (GNC), and provides a comprehensive framework for custom control design for different M-UAV platforms.[5] The navigation module in PX4 fuses measurements from inertial and position sensors to estimate the attitude and position of the vehicle. Based on the guidance strategy and selected vehicle configuration, the autopilot computes the motor signals to achieve a desired setpoint.

PX4 is integrated in the Dronecode environment which enables communication between different modules and hardware using the MAVLink protocol. This allows the use of companion computers in control applications to add additional processing power and integrate additional sensor information, e.g. visual odometry.[1] Recent trends in PX4 integration have exploited the modular nature of the Robot Operating System (ROS) which can be run on companion computers, such as ODROID XU4, the Intel Aero Compute Board, or Raspberry Pi 3. ROS allows the seamless integration of open-source nodes for GNC applications and details on ROS integration with PX4 for swarm control of UAVs can be found in Lamping *et al.*[6]

In this work we follow a simple software architecture without ROS integration as shown in Fig. 6 to

integrate flight and morphing control systems using a Pixhawk 2[i] and Raspberry Pi 3B+[ii] boards for flight control system and companion computer, respectively. The implemented software architecture uses MAVLink protocol to pass information between the FCS and companion computer. Note however that the control approach can be easily extended to a ROS framework using MAVROS.[6]

The morphing mechanism, as also shown in Fig. 6, is driven by the companion computed and can be controlled in either open-loop (dashed arrows) or closed-loop (solid arrows) fashion. In open-loop operation the possible CG offsets Δx_{cg} are pre-computed using Eq. (6) based on user inputs of the mass and location of the multiple payloads. The required morphing angle $\Delta\psi$ is then computed using Eq. (13) assuming no thrust correction, i.e. $\Delta e = 0$. In closed-loop operation the morphing angle is commanded directly to balance the throttle difference between front and rear rotors as discussed in the next section. The Morphing Control System (MCS) has been implemented on the companion computer which also controls the morphing mechanism to sweep the front arms, as discussed in detail in Sec. IV.

B. Cascaded Control Approach for Stability Augmentation

In this section we describe a control strategy for the integration of the FCS with the morphing mechanism for the longitudinal problem assuming the vehicle platform to be symmetric in the x-z plane (cmp. Fig. 2). As shown in Fig. 7, this simplified control problem can be addressed through a cascaded control approach of (a) FCS to stabilize the orientation of the M-UAV by commanding throttle outputs to the rotors, ΔT, and (b) MCS to adjust the morphing angle $\Delta\psi$ to balance the vehicle such that $\Delta x_{cg} = \Delta x_{np}$ and hence $\Delta T = 0$.

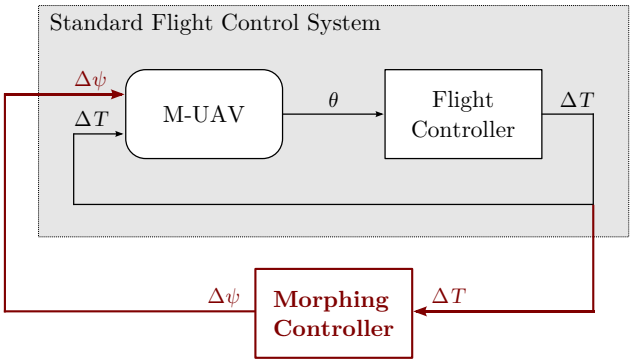

Figure 7: Cascaded control architecture integrating a standard flight controller with a morphing controller for longitudinal pitch stabilization.

The flight control part in the inner loop is not considered in this work and we rely on the standard PX4 autopilot to stabilize the vehicle by reducing the pitch angle θ.[5] If the M-UAV is off-balanced, for example due to a parcel delivery, the compensating actions of the FCS would lead to a mean differential thrust, ΔT, between front and rear rotors, as described in Eq. (9). The objective of the morphing controller in the outer loop in Fig. 7 is to minimize the differential thrust ΔT by manipulating the morphing angle $\Delta\psi$. The outer cascade can be implemented using a simple proportional-integral-derivative (PID) controller or a model-based control approach using Eq. (13) to synthesize the controller.[15] In this work we only consider the longitudinal problem where both motor arms are assumed to move symmetrically. Note however that the control approach can be extended to 3D problems including lateral actuation by decoupling the morphing of the left and right motor arm.

[i] `https://pixhawk.org` (accessed 27 Nov 2018)
[ii] `https://www.raspberrypi.org/products` (accessed 27 Nov 2018)

IV. Proof of Concept for a Morphing Tricopter UAV

In this section we demonstrate the proposed morphing concept for a coaxial Y6 tricopter configuration as shown in Fig. 8. The design of the vehicle follows a novel methodology for the design of heavy-lift multirotor vehicles using coaxial rotors as presented in detail in Ong *et al.*[13] In this paper, we instead present the implementation of the morphing technology and the integration of a morphing controller with an off-the-shelf FCS to demonstrate the benefits of the morphing concept in flight experiments.

This section concludes with final flight test results to evaluate the benefits of the morphing technology. The evaluation will focus on the demonstration of *improved stability* and *optimal operation efficiency* by monitoring the motor outputs for each coaxial rotor:

Improved stability To demonstrate stability of the morphing concept for a specific morphing angle and payload distribution, the motor throttle output level of each coaxial system must be equal while the vehicle is in pitch equilibrium.

Optimal operation efficiency Based on the characterization of the selected motors in Sec. IV.A.1, we can identify an efficient throttle range for hover operation. To demonstrate that the proposed morphing concept leads to more efficient operation, we compare the operating range of all motors for a morphed (balanced) against a rigid (unbalanced) configuration.

(a) CAD design of prototype showing parcels

(b) Actual implementation of prototype

Figure 8: Design and implementation of a morphing Y6 tricopter configuration for multi-parcel delivery with the specifications detailed in Tab. 3.

Table 3: Specifications for prototype system as shown in Fig. 8.

Maximum Take-off Weight	15.2 kg
Empty Take-off Weight (no payload)	9.2 kg
Individual Payload Weight	4×1.5 kg $= 6$ kg
BLDC Motor	R9 6125 330KV
Electronic Speed Controller	X-Rotor Pro 60A
Propeller	2255 Carbon Fibre Propellers
Battery	2 x Li-Po 6S (22.2 V) 5200 mAh 60C
Flight Time (for above batteries)	10 mins

A. Vehicle Design

Figure 8 compares the initial design of the morphing tricopter against the actual implementation of the vehicle with the specifications defined in Tab. 3. The design has the capacity of transporting four Singapore Post XS Parcels (20 x 15 x 9cm) with a payload capacity of 1.5 kg each for multi-parcel delivery. Depending

on the battery selection and payload configuration, the vehicle can hover for up to 10 minutes. Although it has been shown that coaxial propulsion systems are less efficient compared to their single-rotor counterparts and require 22% more power,[16] the proposed prototype system uses three pairs of coaxial 22-inch rotors. By using a coaxial propulsion system, we allow for failsafe redundancy of the M-UAV and achieve a smaller design due to the better thrust-to-volume ratio of coaxial systems.

1. *Approximation of Motor Parameters*

UAVs designed for industrial applications typically use electric brushless DC (BLDC) motors due to their better speed versus torque characteristics, high dynamic response, high efficiency, noiseless operation, and long operating life compared to brushed DC and induction motors.[17] Selecting the right motor is crucial in the design of efficient M-UAVs since all the lifting action is done by the rotors (as opposed to wings on conventional fixed-wing vehicles).

Following the design procedure detailed in Ong *et al.*,[13] the R9 6125 motor[iii] was selected that can produce around 3 kg of thrust each at 50% throttle level. To select suitable and efficient motors, we can refer to manufacturers datasheets to obtain thrust over a specific throttle range and mechanical efficiency which is usually given in gram per Watt. However, the mechanical efficiency does not account for the power losses in the motors which can be obtained either through thrust stand measurements or by computing the electrical efficiency relating the motor input power to the output power. Based on a simplified model and given data in manufacturers' specifications, we can characterize different BLDC motors.[14] For the selected R9 6125 motor, the efficient throttle operating range is between 40% and 70% with the ideal hovering throttle at 53%. With this approximation, the operating throttle range of the M-UAV should be within the specified range of $0.4 \leq e^0 + \Delta e \leq 0.7$ (cmp. Eq. (11)) in order to have better flight endurance and motors longevity.

2. *Flight Control System*

In this work we use the off-the-shelf Pixhawk 2 system to manage all flight aspects of the vehicle.[5] As introduced in Sec. III.A, Pixhawk 2 controls the rotation-per-minute (rpm) of each individual motor to stabilize the vehicle around defined attitude reference conditions using a navigation module and various in-built sensors. The FCS uses a external GPS module to estimate the vehicle position and enable autonomous tracking of waypoints which can be defined as user inputs using a mission planner software.

With Pixhawk 2 calibrated as a Y6 tricopter configuration, the FCS is designed to compensate any balancing issues following a parcel delivery by adjusting the difference in rpm between the front and rear motors. Although this control action leads to inefficient motor operation, the Pixhawk 2 FCS provides the main stabilizing actions and can dynamically correct for external disturbances due to wind. The morphing control system detailed in the next section has been designed as an outer loop controller to sweep the motor arms and provide long-term efficiency gains due to improved stability characteristics.

B. Implementation of Morphing Mechanism

The most important considerations in the design of the mechanism to achieve the sweeping motion of the arms are the additional weight of the mechanism, the change in CG due to the sweeping motion, and the forces acting on the actuators during flight. In this section, we describe the design of the mechanism and elaborate on how the mechanism controller is integrated with the overall FCS.

1. *Design of Morphing Mechanism*

The Y6 configuration shown in Fig. 9a provides the starting point for the design of the morphing mechanism for stability augmentation. Following the concept of multirotor morphing, as introduced in Sec. II, we can symmetrically sweep the front arms to morph the vehicle frame from a Y6 to a T6 configuration and affect the resulting NP location of the rotor forces to re-balanced the vehicle.

In this work we use two Linear Servo Actuators (LSAs) as the main driving force to actuate the morphing mechanism as illustrated in Fig. 9b. Based on a previous design of a morphing mechanism,[18] we found that regular or high-torque servos had multiple drawbacks. Servos have a limited range of rotation of usually up

[iii] `www.4fpv.com/product/277390885` (accessed 4 April 2018)

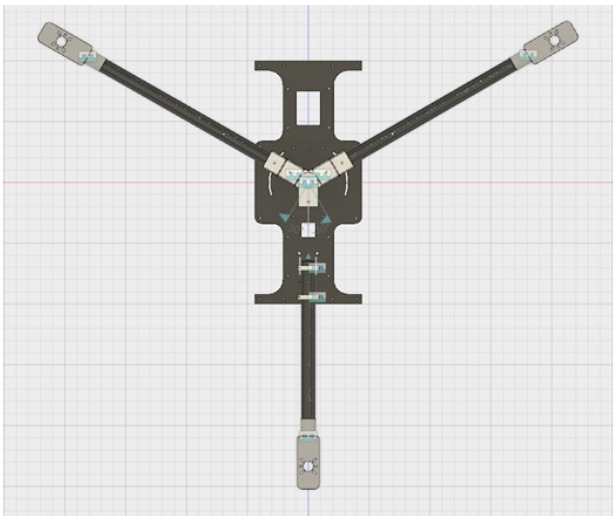

(a) Y6 configuration with rotating front arms

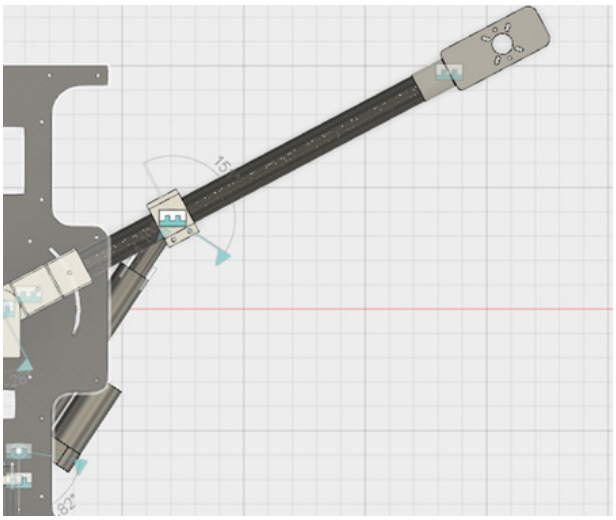

(b) Morphing mechanism with linear servo actuators

(c) Linear servo actuators fully extended and retracted

(d) Actual implementation of morphing mechanism

Figure 9: Design of M-UAV with morphing mechanism using linear servo actuators.

to 90° and, due to their limited applicable torque, require an additional gear which increases the additional weight of the mechanism.

With a maximum push/pull strength of 80 kg over a stroke length of 0.15 m the selected LSAs provide the best compromise for the envisioned morphing mechanism. However, the LSAs have no built-in potentiometer for position control and the extension of the actuator is controlled by a positive voltage input source. To retract the actuator, the polarity of the voltage source must be reversed. Figure 9c shows the LSAs when fully extended and retracted and Fig. 9d illustrates the final implementation of the morphing mechanism.

2. Development of Mechanism Control System

Without position control, the LSAs cannot be integrated directly in the morphing control mechanism. Hence, a four-channel relay module was introduced to work with the morphing controller to enable position control and improve accuracy during a morphing sequence. The relay module acts as an electronically operated switch which can also be used to reverse the current flow into the LSA and cause it to retract.

Figure 10 shows the schematic of the morphing mechanism which comprises of a 4-channel relay module to command the LSAs following control inputs from the Morphing Control System (MCS) implemented on a Raspberry Pi 3B+. The schematic follows the cascaded control architecture as introduced in Figs. 6 and 7

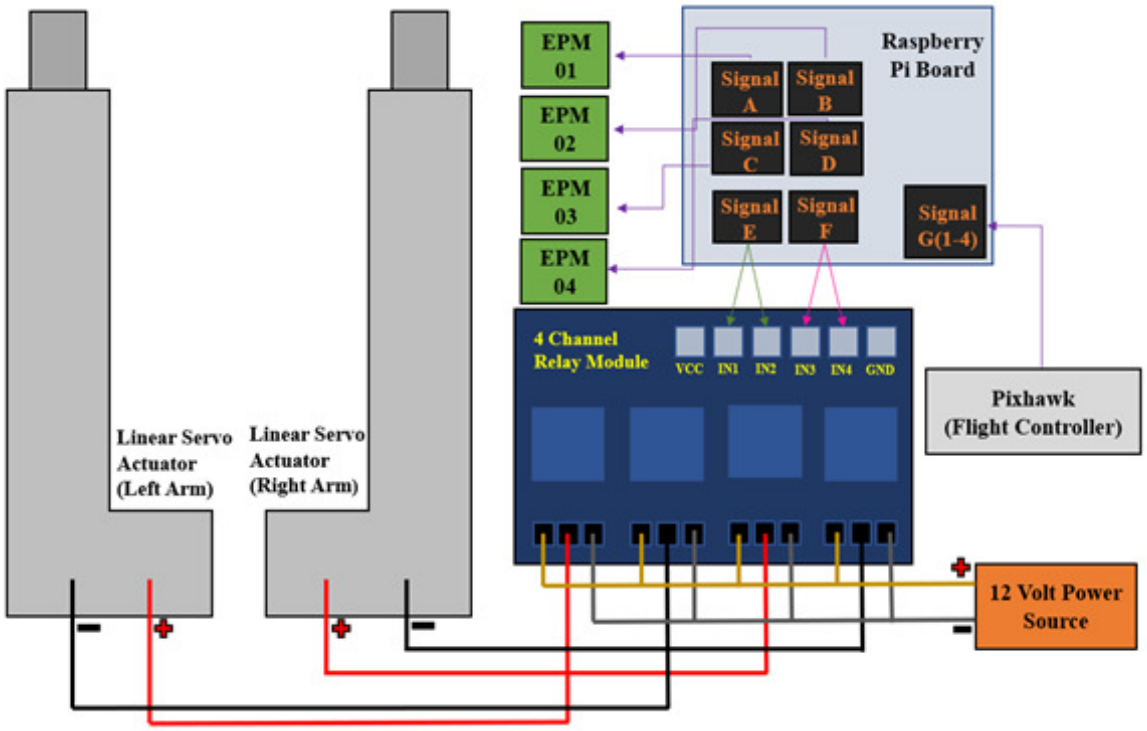

Figure 10: System diagram of integrated morphing control system.

constituting of the morphing mechanism (LSAs), companion computer (Raspberry Pi Board), and flight controller (Pixhawk). Note that the schematic also shows connections to four Electro Permanent Magnets (EPMs) which are used to hold and release the individual payloads.

The MCS has been designed to operate in open-loop or closed-loop fashion to receive information from either user inputs or the Pixhawk flight controller. In this work we only consider the open-loop implementation where a sequence of morphing angles is pre-computed based on the specified sequence of payloads distributions (weight and location of the parcels). Since the proposed morphing concept in Sec. II is based on the morphing angle ψ and the implemented morphing mechanism uses LSAs, we have mapped the actuator stroke length l_{LSA} to the morphing angle based on the geometry shown in Fig. 9.

Based on initial system tests to identify the LSA mechanical specifications we found the average extension speed to be 15.6 mm/s for both LSAs over the entire stroke length. Using this information, the MCS then converts the LSA stroke length l_{LSA} into time delay variables which are used to trigger controlled output signals to activate the relay module to extend or retract the LSAs.

During a flight mission, the Pixhawk FCS system manages the navigation of waypoints, as described in Sec. IV.A.2, and triggers the morphing sequence once the vehicle has landed and delivered a parcel. Note however that the control architecture can be extended to operate in a closed loop fashion and control the morphing angle based on the difference in commanded motor throttle outputs by the Pixhawk FCS.

3. Validation of Mechanism Control System

To validate the morphing mechanism to track the desired morphing angle ψ, the vehicle was tested in a static position and the desired morphing angles ψ_c were commanded using the user interface and morphing mechanism control system shown in Fig. 10. The mechanism tests were conducted from the minimum limit of implemented morphing mechanism from $\psi = 10°$ to $\psi = 50°$ in increments of 5°.

The actual morphing angles of the left and right motor arm, $\tilde{\psi}_l$ and $\tilde{\psi}_l$, respectively, were then measured and compared against the commanded morphing angles as shown in Fig. 11. The slight differences in angles between the left and right motor arms were due to both LSAs having slightly different extension speeds of 15.5 mm/s and 15.7 mm/s, respectively. However, such small errors in morphing angles, as shown in

Fig. 11b, are compensated by the FCS and have negligible effect on the flight performance.

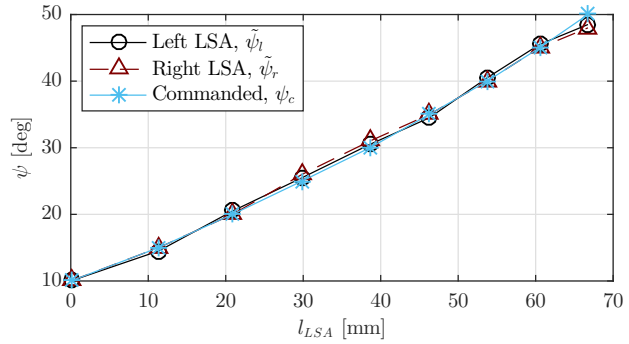

(a) Commanded and actual morphing angles against stroke length

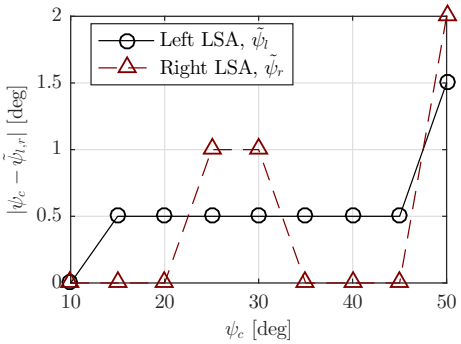

(b) Errors in actual morphing angles against commended angles

Figure 11: Comparison of commanded morphing angle ψ_c versus actual morphing angles for left and right Linear Servo Actuator (LSA), $\tilde{\psi}_l$ and $\tilde{\psi}_l$, respectively, as a function of LSA stroke length l_{LSA}.

C. Flight Test Results

Three flight tests as defined in Tab. 4 were conducted to demonstrate the benefits of the proposed morphing technology on the overall vehicle flight performance. All flights are in hover mode and the motor outputs have been monitored over the duration of each flight lasting approximately 2 mins each. Figures 12-13 show examples of the throttle outputs of the lower motors of each rotor for all three flight cases as commanded by the FCS. Note that the lower motors in coaxial rotors tend to spin slightly faster compared to the upper motors to compensate for the aerodynamic interactions between both propellers.[16]

Table 4: Mission profile for three flight tests.

Flight	Mission profile	Morphing angle
1	No payload (Flight data used for referencing)	$\psi = 30°$
2	1.4 kg Payload at payload bay maximum rear position	$\psi = 30°$
3	1.4 kg Payload at payload bay maximum rear position	$\psi = 18°$

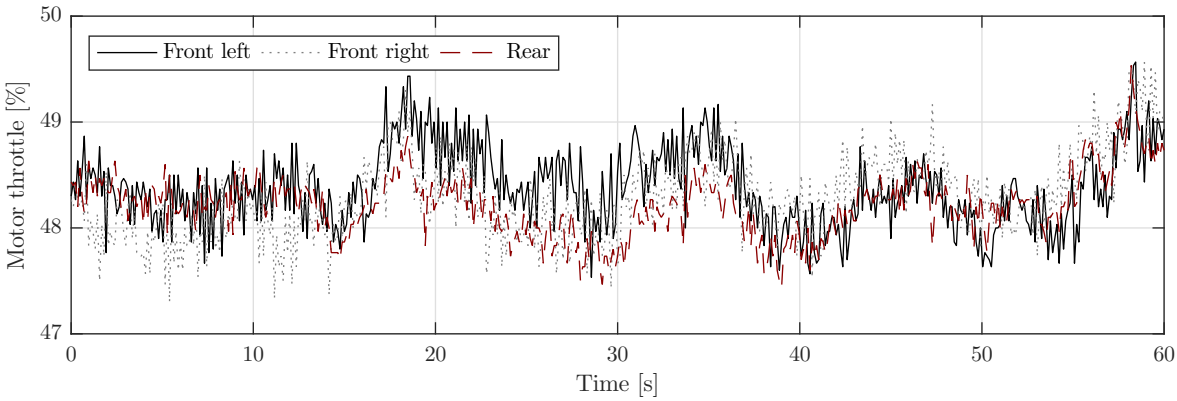

Figure 12: Pixhawk log data of commanded motor throttle outputs in percentage of max throttle for the lower front left, front right and rear motors for Flight 1 as defined in Tab. 4.

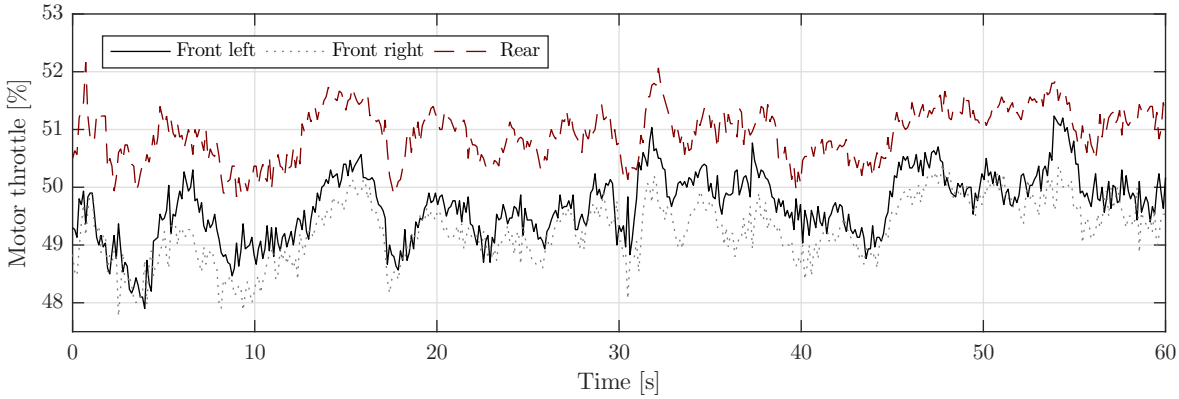

(a) Flight 2 (without morphing)

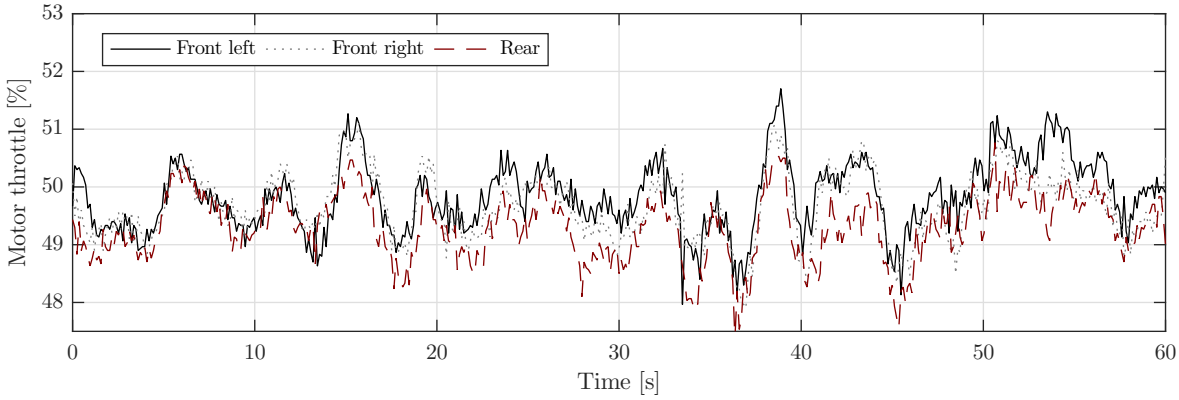

(b) Flight 3 (with morphing)

Figure 13: Pixhawk log data of commanded motor throttle outputs in percentage of max throttle for the lower front left, front right and rear motors for Flights 2 and 3 as defined in Tab. 4.

The first flight without payloads in Y6 configuration with $\psi = 30°$ serves as a benchmark case. As the (empty) vehicle is designed to be balanced for this configuration, we expect all motor outputs to be approximately balanced and the motor output for Flight 1 shown in Fig. 12 are used as reference data to evaluate the morphing concept.

To demonstrate the effect of an unbalanced configuration and the benefits of morphing, a payload of 1.4 kg was attached to the rear payload bay of the vehicle and the hover tests were repeated without (Flight 2) and with (Flight 3) morphing to compare the motor outputs in both cases as shown in Fig. 13. The rear payload bay is located 281 mm aft of the axis of rotation for the motor arms (origin of the reference frame defined in Fig. 2). Using Eq. (6) this leads to an overall CG offset of 0.05 m for the unbalanced vehicle configuration considering an arm length of $l = 0.4$ m. From the flight data in Fig. 13a corresponding to Flight 2 (without morphing), it is obvious that for the unbalanced configuration the FCS commands the rear motor to spin faster compared to the two front motors to compensate for the additional weight at the rear and to stabilize the vehicle.

Flight 3 was performed with the same payload configuration as Flight 2, but the motor arms have been morphed from $\psi = 30°$ to $\psi = 18°$ to compensate for the CG offset of 0.05 m using Eq. (13). Figure 13b shows the motor output efficiency for Flight 3 indicating that the rear motor is commanded to produce a lower output compared to the front motors. Hence, after morphing the motor outputs are similar to Flight 1 demonstrating that the FCS no longer needs to compensate for the additional weight at the rear which leads to a more balanced thrust distribution between front and rear rotors.

The flight data in Figs. 12-13 only presents details of all flight tests, however, averaging over all flight data as shown in Fig. 14 indicates a similar trend. For the benchmark test (Flight 1), the vehicle is well

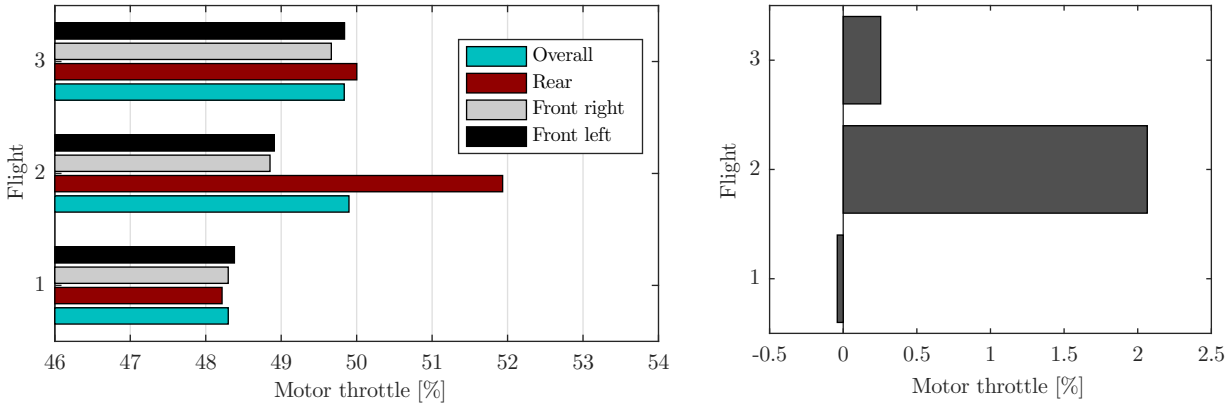

(a) Absolute throttle outputs

(b) Difference between front and rear throttle outputs

Figure 14: Mean motor throttle output in percentage of max throttle for the Flights 1, 2 and 3 as defined in Tab. 4.

balanced and the overall throttle levels are 48% which lies in the desired region of 40-60%.[16] As shown in Fig. 14a, the overall throttle levels only increase to 50% when the payload is added (Flights 2 and 3) due to high thrust-to-weight ratio of the vehicle which is designed to carry a total of 6 kg payload. However, comparing the difference in mean throttle output levels between both front rotors and the rear rotor for all flight tests, as shown in Fig. 14b, we can see that the throttle bias has decreased from 2% for Flight 2 to 0.2% for Flight 3. This indicates that the morphed configuration is more balanced along the longitudinal axis compared to Flight 2 without morphing which improves the vehicle stability and should lead to longer flight times.

V. Conclusions

The proof-of-concept in this paper demonstrates that the flight characteristics of a multirotor UAV with variable payload distribution can be enhanced by morphing the vehicle airframe. Morphing the geometry of a conventional multirotor airframe enables the vehicle to continuously adjust its neutral point to match varying center of gravity positions. This allows a UAV to carry and deliver multiple parcels without deteriorating its flight characteristics.

The proposed morphing has been implemented and tested for a coaxial Y6 tricopter configuration using linear servo actuators to manipulate the motor arms. By integrating the morphing controller with existing flight control systems in a cascaded control approach, it was shown that the morphing controller can progressively improve the vehicle stability by balancing the throttle outputs of front and rear rotors. Flight test results demonstrated that the proposed morphing mechanism can completely re-balance slight CG offsets causing all rotors to operate at the same throttle setting. Hence, the morphing approach can be used to optimize the performance of all rotors on the vehicle subject to varying payload positions.

Although the morphing concept has only been demonstrated in this work for a tricopter configuration, the approach easily expands to longitudinal and lateral morphing of general multirotor configurations such as quadrotors. In this work the bandwidth of the morphing mechanism is limited by the linear servo actuator but in theory the morphing concept can be used to stabilize the drone in the presence of dominant wind disturbances.

Acknowledgments

The invention/technology presented in this paper is the subject of patent protection for which there is a patent pending.

References

[1]Brunner, G., Szebedy, B., Tanner, S., and Wattenhofer, R., "The Urban Last Mile Problem: Autonomous Drone Delivery to Your Balcony," *ArXiv e-prints*, Vol. 1809.08022, Sept. 2018, https://arxiv.org/abs/1809.08022.

[2]Stengel, R. F., *Flight Dynamics*, Princeton University Press, Princeton, NJ, USA, 2015.

[3]Liu, Y., Kreimeier, M., Stumpf, E., Zhou, Y., and Liu, H., "Overview of recent endeavors on personal aerial vehicles: A focus on the US and Europe led research activities," *Progress in Aerospace Sciences*, Vol. 91, may 2017, pp. 53–66.

[4]González, I., Salazar, S., Torres, J., Lozano, R., and Romero, H., "Real-Time Attitude Stabilization of a Mini-UAV Quad-rotor Using Motor Speed Feedback," *Journal of Intelligent & Robotic Systems*, Vol. 70, No. 1-4, aug 2012, pp. 93–106.

[5]Meier, L., Tanskanen, P., Heng, L., Lee, G. H., Fraundorfer, F., and Pollefeys, M., "PIXHAWK: A micro aerial vehicle design for autonomous flight using onboard computer vision," *Autonomous Robots*, Vol. 33, No. 1-2, feb 2012, pp. 21–39.

[6]Lamping, A. P., Ouwerkerk, J. N., Stockton, N. O., Cohen, K., Kumar, M., and Casbeer, D. W., "FlyMASTER: Multi-UAV Control and Supervision with ROS," *Aviation Technology, Integration, and Operations Conference, AIAA AVIATION Forum*, Atlanta, GA, USA, jun 2018.

[7]Czyba, R., Szafranski, G., Janik, M., Pampuch, K., and Hecel, M., "Development of co-axial Y6-Rotor UAV - Design, mathematical modeling, rapid prototyping and experimental validation," *IEEE International Conference on Unmanned Aircraft Systems (ICUAS)*, Denver, CO, USA, 2015.

[8]Barbarino, S., Bilgen, O., Ajaj, R. M., Friswell, M. I., and Inman, D. J., "A Review of Morphing Aircraft," *Journal of Intelligent Material Systems and Structures*, Vol. 22, No. 9, 2011, pp. 823–877.

[9]Blondeau, J., Richeson, J., and Pines, D., "Design of a Morphing Aspect Ratio Wing Using an Inflatable Telescoping Spar," *44th AIAA Structures, Structural Dynamics, and Materials Conference*, Norfolk, VA, USA, 2003.

[10]Prabhakar, N., Prazenica, R. J., Gudmundsson, S., and Balas, M. J., "Transient Dynamic Analysis and Control of a Morphing UAV," *AIAA Guidance, Navigation, and Control Conference*, San Diego, CA, USA, jan 2016.

[11]Riviere, V., Manecy, A., and Viollet, S., "Agile Robotic Fliers: A Morphing-Based Approach," *Soft Robotics*, Vol. 5, No. 5, oct 2018, pp. 541–553.

[12]de Angelis, E. L., "Stability analysis of a multirotor vehicle hovering condition," *Aerospace Science and Technology*, Vol. 72, jan 2018, pp. 248–255.

[13]Ong, W., Srigrarom, S., and Hesse, H., "Design Methodology for Heavy-Lift Unmanned Aerial Vehicles with Coaxial Rotors," *AIAA Science and Technology Forum and Exposition*, San Diego, CA, USA, 2019.

[14]Gabriel, D. L., Meyer, J., and du Plessis, F., "Brushless DC motor characterisation and selection for a fixed wing UAV," *IEEE Africon*, sep 2011.

[15]Wood, T. A., Hesse, H., and Smith, R. S., "Predictive Control of Autonomous Kites in Tow Test Experiments," *IEEE Control Systems Letters*, Vol. 1, No. 1, jul 2017, pp. 110–115.

[16]Bondyra, A., Gardecki, S., Gąsior, P., and Giernacki, W., "Performance of Coaxial Propulsion in Design of Multi-rotor UAVs," *Challenges in Automation, Robotics and Measurement Techniques*, Springer, Switzerland, 2016, pp. 523–531.

[17]Yedamale, P., "Brushless DC (BLDC) Motor Fundamentals," Tech. Rep. DS00885A, Microchip Technology Inc., Chandler, AZ, USA, 2003.

[18]Cheng, D., Ong, W., Charles, A. C., Hum, B., Ho, N., Hogan, G. E., Tan, J., Ibrahim, I. H., Hesse, H., and Srigrarom, S., "Development of a VTOL Flying Car Concept," *International Conference on Intelligent Unmanned Systems (ICIUS)*, Jeju, South Korea, Aug. 2018.